2. ACTUATOR DEVELOPMENT

2.1 Introduction

The University examined the design of actuators for both SDOF and MDOF active microgravity isolation systems. For SDOF systems, two actuators were considered: a special large gap magnetic actuator and a large stroke Lorentz actuator. The magnetic actuator was viewed to be of greater difficulty than the Lorentz actuator with little compelling technical advantage and was dropped from consideration. A Lorentz actuator was designed and built for the SDOF test rig using magnetic circuit and finite element analyses. This design and some experimental results are discussed below.

The University also examined the design of actuators for MDOF isolation systems. This includes the design of an integrated 1 cm gap 6–DOF noncontacting magnetic suspension system and of a "coarse" follower which permits the practical extension of magnetic suspension to large strokes. The proposed "coarse" actuator was a closed kinematic chain manipulator known as a Stewart Platform. The integration of the two isolation systems together, the isolation tasks assigned to each, and possible control architectures were also explored. The results of this research are examined in Section 3.

2.2 Large–Stroke Lorentz Actuator and Test Results

A compact large–stroke Lorentz actuator was designed, built, and tested at the University of Virginia The requirements for the laboratory prototype were a total stroke of two inches and enough force capability to isolate a mass of 75 lbs. connected by an umbilical (air dashpot) to a source generating very low frequency vibrations. Force linearity with current and independent of position were also desirable. Moreover, in view of the ultimate goal of deployment in space, such a device had to be compact and lightweight. Low power consumption and low heat generation during operation were also important. A design was carried out using a simple computer program based on magnetic circuit analysis. The initial design required a 3.2 inch diameter ring magnet of very high maximum energy product (35

mega–Gauss–Oersted). This design was not only large and heavy, but could not be built from a single piece since magnet manufacturers do not make sizes larger than 2 inches. The cost and difficulty of assembly ruled out an actuator using multiple magnet segments. It therefore became necessary to design the Lorentz actuator using a smaller core gap than is conventionally used. Usually this gap is large to reduce magnetic flux leakage across it so as to yield an actuator that will produce a force independent of coil position. It was hypothesized that this leakage could be substantially reduced by saturating the actuator's core. This could only be verified, short of building a prototype, via finite element analysis. A commercially available finite element analysis package, MAGGIE,

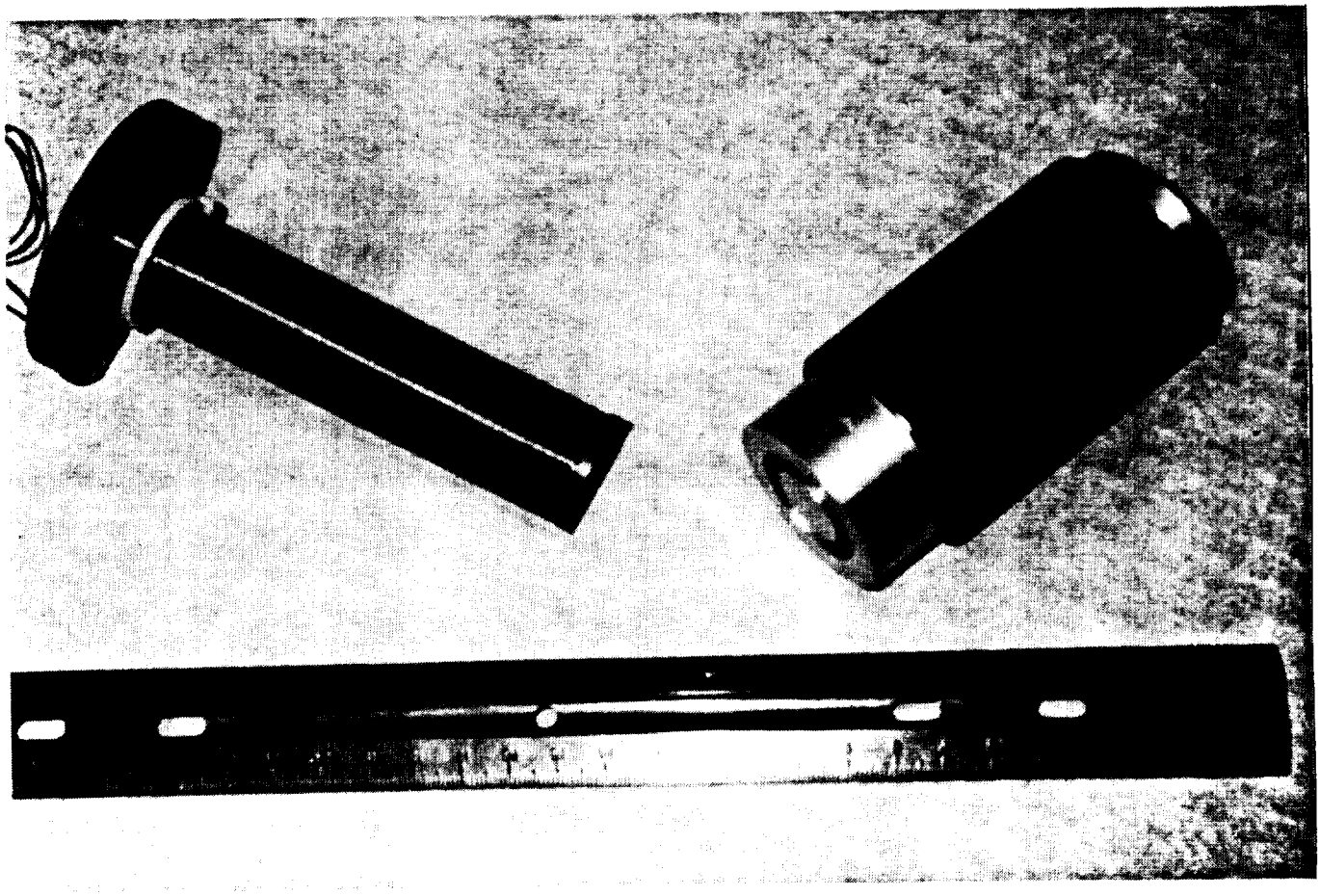

Figure 1: Large–stroke Lorentz actuator

was used to "test" a large number of designs. The final actuator, shown in Figure 1, has an outer diameter of 1.95 inches and a 4 inch length. This actuator has the following features [1]:

* **Long Stroke:** The actuator has two inches of stroke.
* **Position Independence:** Over the entire stroke, the actuator's gain is almost independent of position. For a constant coil current, this means that the actuator force is the same irrespective of the axial position of the coil. This is achieved by the design since the maximum flux density across the core gap is only 7% of the maximum flux density across the pole face gap.
* **Current Linearity:** The average flux density in the effective air gap remains constant with variations in the coil current between the upper and lower limits. This is achieved through the large reluctance of the permanent magnet in the electromagnetic flux circuit and the saturation of the core.
* **Force:** A maximum force of 1.50 lbs is produced by this actuator with a coil current of 2.5 A.
* **Materials:** The permanent magnet is neodymium iron boron, which has a very high maximum energy density product of 35 MGOe. The circuit material is a high permeability nickel–iron alloy that saturates at 1.50 Tesla. These materials permit a compact design.

The experimental results have confirmed the soundness of the design approach [1]. Figure 2a shows the actuator force plotted versus position for a number of values of coil current. Note that the actuator's force is fairly independent of the coil position over the actuator's operating range (0.5 to 2.5 inches). Note also that the actual forces are larger than the predicted forces, but still within 20%. Figure 2b shows the same data in terms of actuator force plotted versus coil current for different positions. As shown in the figure, the actuator has a high degree of linearity with respect to current. Note that the actuator gain (slope of the line in Figure 2b) is fairly independent of coil position and is approximately 0.6 lbf/amp.

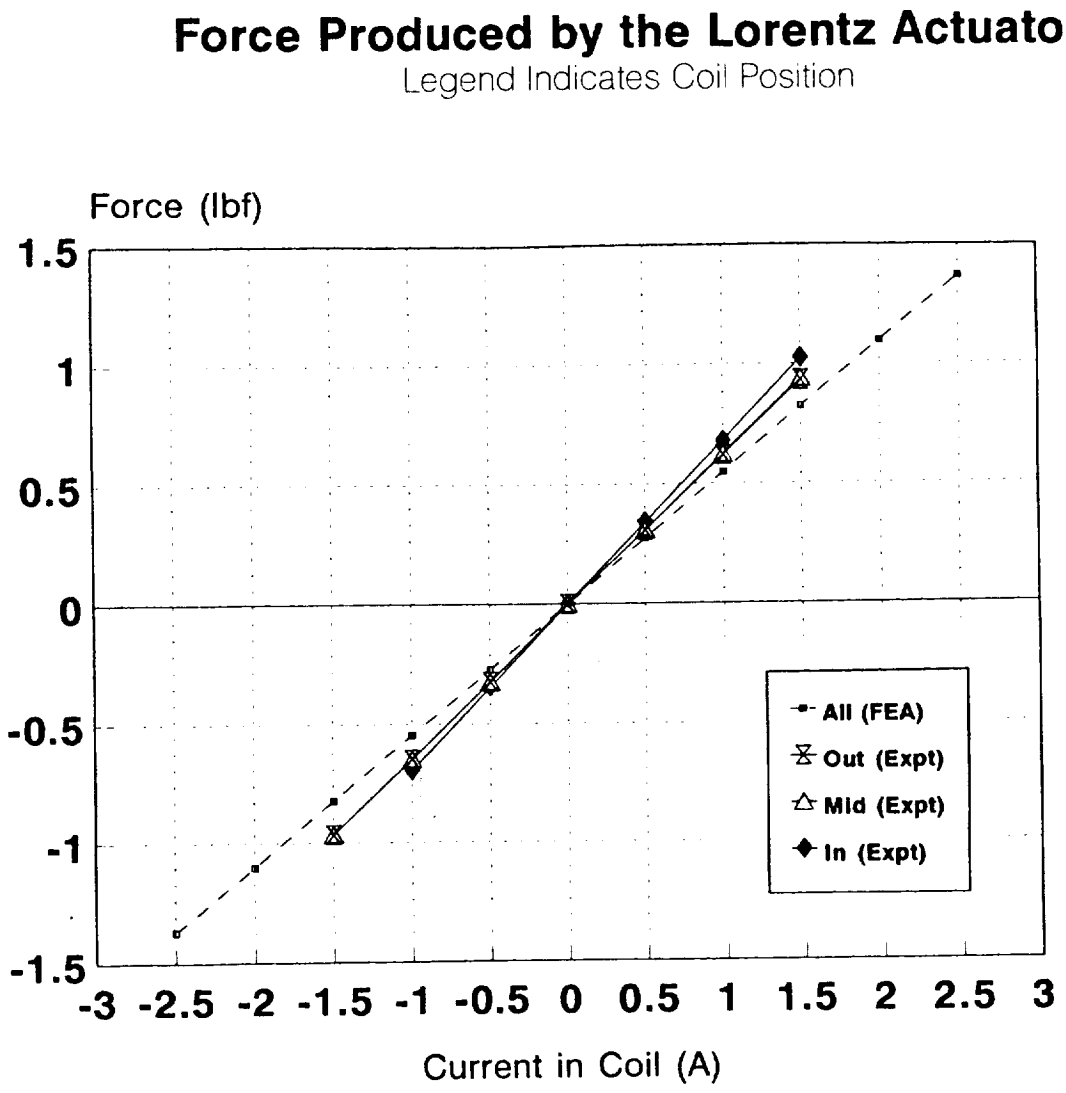

Figure 2: Actuator force vs. current.

3. MULTIPLE DEGREE OF FREEDOM ACTUATOR DESIGN

3.1 Introduction

The University of Virginia also examined the design of multiple–degree–of–freedom actuators for microgravity vibration isolation. The fundamental constraint on isolation performance to be considered during actuator design is the available working envelope [2,3]. The implications of this constraint on active isolation were examined by the University in two journal publications [2,3].

Figure 3 shows the relationship between the envelope (peak–to–peak displacement and frequency for several sustainable RMS acceleration levels [4]. The graph is for a

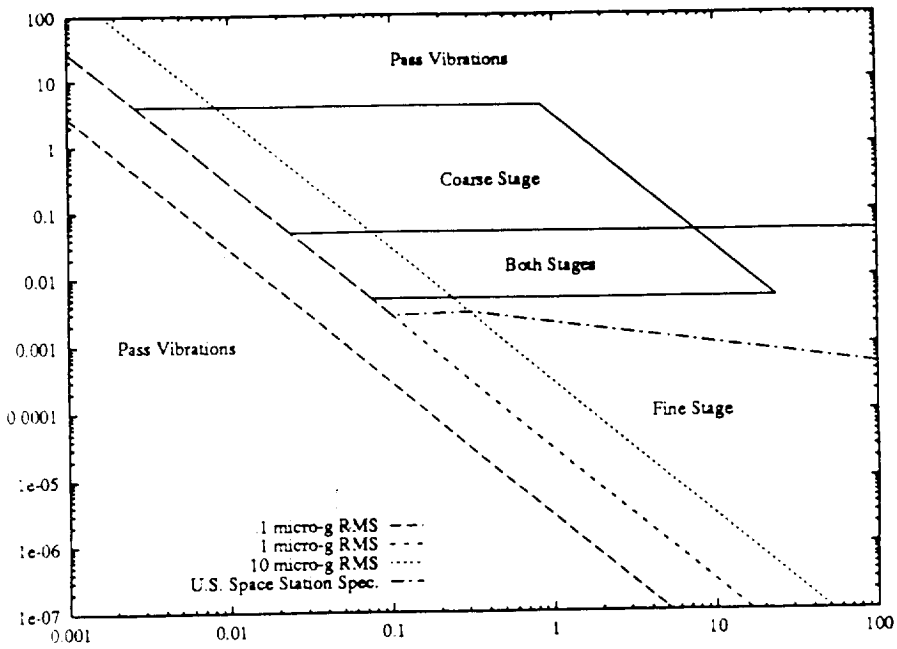

Figure 3: Peak–to–peak displacement vs. frequency

one–degree–of–freedom case and assumes sinusoidal vibrations, but the relationships are acceptable for order of magnitude estimates even if these assumptions are relaxed. No definitive specification of the required isolation levels or frequency range exists. The proposed US Space Station usable specification is also shown in Figure 3. It is claimed that vibrations below this curve will not adversely affect microgravity experiments. The design examined in

this section is an active isolation system with a "reasonable" envelope of 4 inches of travel and a sustained 1 ug RMS residual acceleration. It can be seen from the figure that this will offer isolation down to 0.002 Hz. The amplitude to which vibrations can be attenuated is constrained only by controller design and available instrumentation. Operation at lower frequencies, however, requires a larger envelope, which becomes prohibitive in terms of available spacecraft space. Another specification for the six–degree–of–freedom system considered is a rotational range of 40 degrees.

A redundant coarse–fine scheme with magnetic suspension was chosen. This design is particularly attractive for microgravity applications since it allows the use of magnetic suspension while overcoming range–of–motion limitations. The design uses a Stewart platform for the coarse stage and a novel magnetic bearing for the fine stage [4,5]. The approximate regions of activity in the frequency–displacement plane of these two devices are also shown in Figure 3. Both stages act to attenuate spacecraft vibrations, effectively reducing vibration amplitudes below their active regions on the displacement vs. frequency plane. As an example, it can be seen in the figure that a vibration of the spacecraft with 10 inches of displacement at a frequency of 1 Hz falls outside the active region and could only be partially attenuated. It should be noted that such a large vibration is unlikely. If the displacement was only 1 inch, however, the coarse stage would absorb all of it except about 0.005 inches, and the remainder would be reduced down to the micro–g level by the fine stage.

The combination of the Stewart platform and a magnetic bearing allows continuous isolation at frequencies above 0.002 Hz, and a compact, reliable package suitable for the application. These choices and some preliminary design concepts are discussed below in detail after a survey of other candidate designs.

3.2 Survey of Published Designs

Several designs for 6 DOF levitation are discussed in the literature. While these designs do not have the envelope of the proposed coarse–fine design, they might be suitable if a

coarse stage is not required. They also deserve examination as alternative designs for the fine stage. A comparison of the specifications for these designs is given in Table 1.

Group	Trans.	Rot.	Force	Envelope	Mass	Actuator	Sensor
Honeywell	5 mm	$\pm 1.6^\circ$	43 N	27x34x50cm	36kg	Mag. Brng.	Eddy & Flux
N. Wales	± 5 mm	$< \pm .2^\circ$	.04 N[a]	100x100x100cm[b]	?	Lorentz	Capacitive
NASA	± 4 mm	$\pm 3^\circ$ [c]	445 N	30x30x15cm[c]	?	Mag. Brng.	Eddy
SatCon	± 10 mm	$\pm 8^\circ$ [c]	4 N	40x40x12cm[c]	4.9kg	Lorentz	Eddy
IBM	± 5 mm	$\pm 4^\circ$	32 N	25x25x15cm[c]	?	Lorentz	Optical
Toshiba	± 2 mm	$\pm 1.5^\circ$	20 N[c]	25x25x20cm	8kg	Mag. Brng.	Eddy

[a] Requirement, not limitation
[b] Includes experiment package
[c] Estimated by authors

Table 1: Comparison of Published Designs

Four designs specifically for microgravity isolation have been published. Honeywell has a well–developed system called FEAMIS [6] with which they have demonstrated impressive isolation performance. The system is designed for the Space Shuttle experiment configuration. The University College of North Wales also has a well–developed system [7] designed for the European Space Agency experiment configuration. NASA [8] has a well–tested laboratory system and has done testing in a weightless environment aboard an aircraft in a parabolic trajectory. They also have demonstrated impressive isolation performance for a feedforward control system. SatCon [9] also has a laboratory magnetic suspension system.

Two actuator designs were developed for different applications, but they are mentioned here because they are similar and could be easily adapted to the isolation application. IBM [10] has a laboratory levitated robot "wrist" which enhances robot accuracy and performance.

Toshiba [11] has a satellite antenna pointing system which is fully developed. Both devices have demonstrated positional accuracies on the order of 1 μm.

Isolation of vibrations with large amplitudes – typically occurring at low frequencies – requires a large translational range. SatCon's system has the largest range, but there is a significant tradeoff with the device's force capability. A coarse–fine approach would allow both a large range, provided by the coarse stage, and a high force capability, since the levitation gaps are small. There is no available data on the rotational range requirements of the application. Isolation with an umbilical disturbance may require a high force capability, as is offered by the systems from Honeywell, NASA, IBM, and Toshiba. Volume and weight should be minimized in any spacecraft. SatCon's, IBM's, and Toshiba's systems offer advantages in envelope volume and weight.

The choice of the actuator technology between Lorentz force and magnetic bearings for MDOF isolation systems is not a clear one. Lorentz actuators offer linearity, simplicity, open loop neutral stability, and compactness. Magnetic bearings offer higher force capability and lower power consumption, particularly if gaps are minimized.

Four position sensor technologies offer promising performance. Eddy current position probes are simple and robust, but bulky and heavy for large gaps. Capacitive sensors are simple and lightweight, but can be noisy in unconstrained environments. Optical lateral effect photo–diodes are compact and quiet, but they require substantial supporting electronics. Hall effect flux sensors can be used with magnetic bearing designs both to linearize the control problem and to measure position.

3.3 Coarse Stage

The Stewart platform is a six degree–of–freedom parallel manipulator which has been used extensively in aircraft cockpit simulator applications. Figure 4 shows the mechanism in the proposed configuration [4]. Six linear actuators (legs) connect a base (bottom) to a platform (top). The base would be mounted in the spacecraft and move with it, while the

platform would track an inertial reference frame. Stepper motor driven ball lead–screws are proposed as actuators.

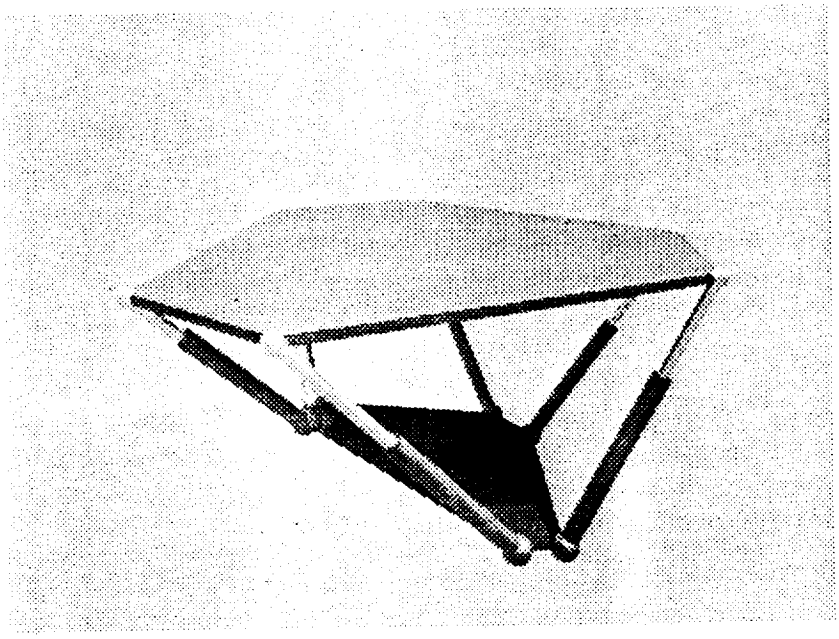

Figure 4: Coarse stage isolation actuator

This mechanism was chosen over other candidates such as a carriage/gimbal assembly, or a serial linkage mechanism, because it has the following features:

* **Inherent rigidity:** The parallel connection of the actuators gives the mechanism rigidity on the order of the extensional rigidity of the actuators. For the proposed actuators, this will allow controller design to ignore the dynamics of the mechanism. The effects of "umbilical" connection to the platform will also be negligible.
* **Determinate inverse kinematics:** The actuator lengths required to achieve a prescribed orientation are found directly from a coordinate transformation from the base to the platform frame. This is seldom the case for a serial linkage. This will also simplify control.

* **Compactness:** The configuration proposed here places the fine stage on top of the platform for convenience in testing. A fully developed implementation could locate the fine system and microgravity experiment in the space between the base and platform, resulting in a compact package.

The Stewart platform has some disadvantages that must be considered. It is nonlinear in its response to actuator lengths, its general direct kinematics have not been discovered in closed form, and it has singularities in its operational space. The first two problems can be overcome with digital controls. The singularities, which are points or loci where the mechanism gains a degree of freedom and the actuators can lose control of the platform, must be addressed by the design.

A simulation code has been written to allow exploration of the design alternatives. Results indicate that our specification (4 inches translation, 40 degrees rotation) will be achievable with actuators 10.5 inches long in the retracted position, and with 9 inches of stroke. The simulations have confirmed that singularities are safely outside the working envelope. Commercial actuators with the required range, load capacity, speed and acceleration have been identified.

3.4 Fine Stage

The magnetic bearing proposed has two parts: a stator which is attached to the Stewart platform, and a surrounding "flotor" to which the experiment is attached. The proposed stator [5] is illustrated in Figure 5. It has twelve pole pieces and coils arranged around the surface of a cube. The cube and pole pieces are ferromagnetic. Each pair of pole pieces and the region of the cube to which they are attached comprise a typical "horseshoe" electromagnet causing an attractive force toward the nearby flotor. Magnetic flux through the center of the cube causes an imbalance in the flux levels of a pair of pole pieces, resulting in a net torque on the flotor.

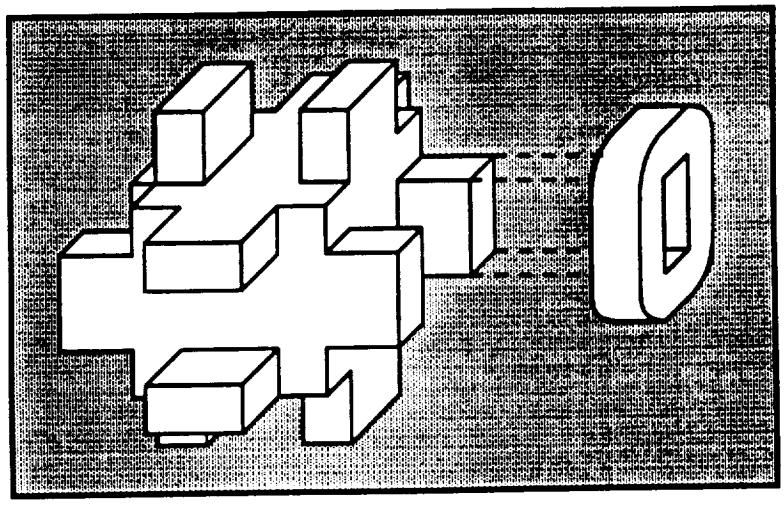

Figure 5: Fine stage isolation stator

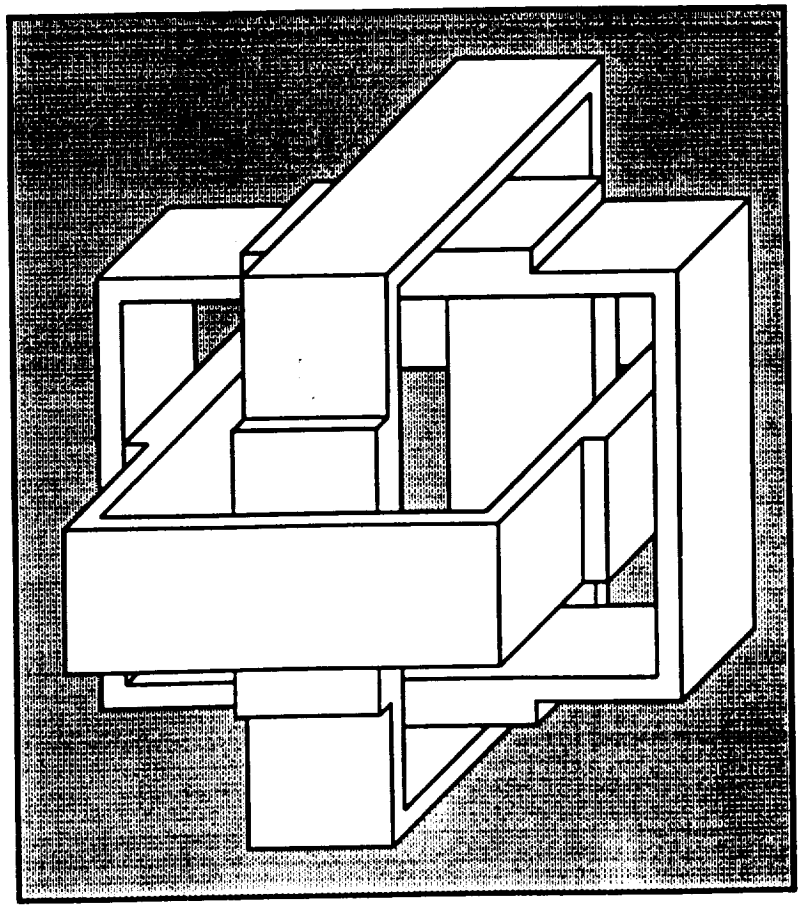

Figure 6: Fine stage isolation flotor

In the proposed design differential Hall effect sensors are located in the base of each pole piece to measure the local flux. All electrical connections will be to the stator.

The flotor concept is illustrated in Figure 6. Three ferromagnetic bands are rigidly attached to each other, but form independent flux paths. The bands are thicker in the region near the pole pieces to avoid saturation. Flux which passes through the center of the cube is returned through the remaining portions of the bands.

Four mounting posts are attached to corners of the cube, and pass through clearances in the flotor. These posts could carry cooling fluid to be circulated through the stator if it is required.

This configuration was chosen over other suspension approaches such as Lorentz actuators or magnetic actuators located on the periphery of the experiment package because it has the following advantages:

* **Compactness:** The high force capability of the magnetic bearing relative to a Lorentz actuator of similar size and power consumption suits the application. Testing in earth gravity will be facilitated, and suspension during launch to protect sensitive instrumentation may be feasible. Also, the rigid structure required to mount actuators around the periphery is avoided.
* **Force/torque balance and rotational range:** Actuators capable of the required forces mounted on the periphery of the experiment are capable of torques far greater than is required, and they limit the rotational range of the experiment. The proposed design approach brings the relative force/torque magnitudes closer to the requirement, and allows substantial rotational range.
* **Integral sensor capability:** Compact semiconductor magnetic flux sensors (Hall effect or magneto–resistive) can be utilized both to stabilize the system and to infer relative position. No elegant integrated approach is known for Lorentz actuators.

3.5 Predicted Performance

The specific design examined at the University has a center cube of 2 in. on a side, pole faces of 1 x .5 in., and pole length of 2 in. Maximum current is determined by allowing a coil current density of 5000 amp/in^2 which is known to be conservative from previous designs. The gap in the centered position was chosen to be .125 in. plus an allowance of .030 in. for inclusion of flux sensors and a protective layer on the inside of the bands. The resulting performance of the design is presented in Table 2. The 53 N force is a continuous worst case, with the stator moved away from the flotor in the direction of the force. The continuous force capability in the centered position is 175 N. Intermittent force capability is limited only by the current capability of the amplifiers, and the saturation limit of the magnetic material used. Using Vanadium Permandur with this design would enable 1000 N force before saturation. Of the 4.5 kg mass, the flotor comprises only 1.2 kg.

Trans.	Rot.	Force	Envelope	Mass
+3.2 mm	+7^o	53 N	15x15x15 cm	4.5 kg

Table 2: Specification of UVA Design

When compared with the designs presented in Table 1, the UVA design has several advantages. The envelope is substantially smaller than any of the previous designs, while the performance is similar. In addition to saving space, this compactness allows the flotor to be naturally rigid, and thus avoids control problems with structural dynamics. The design is lighter than other designs for which data were available [5,6].

4. CONTROL SYSTEM DESIGN ISSUES

4.1 Introduction

The control issues of active microgravity vibration isolation were another area of investigation at the University. The thrust of this research has been the design of feedback/feedforward controllers using modern control synthesis. As part of this investigation we also examined passive vibration isolation analogies. In addition, a control architecture for the six–degree–of–freedom actuator discussed in the last section was proposed.

Active isolation systems for microgravity and pointing applications have been designed and constructed by many investigators. These systems generally use conventional PD control of a noncontacting actuator, either Lorentz or electromagnetic, to achieve low frequency disturbance attenuation. While an actual microgravity experiment may require umbilicals, the isolation systems designed and tested so far cannot provide isolation for such an experiment. These systems achieve their performance by the very low stiffness made possible by low gain feedback of the relative position of the experiment to the experiment rack. Without an umbilical, this stiffness may be set by the designer at will. However, when an umbilical is present, the umbilical stiffness presents a lower bound on achievable stiffness unless the feedback loop is used to introduce a negative stiffness. The University has concentrated its work on the design of control systems for the generic (i.e. with umbilical) microgravity isolation problem. The University has set the following specifications for an active microgravity isolation system [12]:

(1) Unity transmissibility from D.C. to 0.001 Hz so as to prevent the experiment from impacting its enclosure's walls.

(2) At least 40 dB attenuation above 0.1 Hz.

(3) Both stability and performance robustness with respect to changes in umbilical experiment properties, non–collocation or misalignment of sensors and actuators, center–of–mass uncertainties, and unmodeled cross coupling between the degrees of freedom.

Robustness refers to the ability of the control system to perform satisfactorily when the true plant varies from the nominal plant. Performance requirements of the type (2) for rotational degrees of freedom have not yet been specified by NASA or microgravity users, to our knowledge.

4.2 Passive Isolation: An Analogy

The design of an active vibration isolation system for microgravity space experiments was examined from an analogy to passive isolators [12]. It should be noted that the primary reason for pursuing an active rather than a passive system is not the increased flexibility in loop shaping accompanying active control, but the limitations of passive isolation systems. The stiffness of the umbilical precludes achieving a soft enough support so as to meet the isolation requirements for indirect (transmitted through the umbilical) disturbances. Also, a passive isolation system cannot isolate the payload from both indirect and direct (onboard the experiment) disturbances. An active system allows these limitations to be overcome. For example, an active system permits the insertion of a negative stiffness spring in parallel with the umbilical. Note, however, that this approach, i.e. lowering the stiffness, requires the near cancellation of the umbilical's stiffness with that introduced via feedback. If the negative stiffness exceeds that of the umbilical, the equivalent stiffness of the system will be negative and the system will be unstable. It is not surprising then that the introduction of negative stiffness via the controller has no robustness whatsoever. A focus on equivalent stiffness in isolation system design thus leads to control systems which sacrifice robustness for performance. In addition, a design which achieves isolation through lowering the system stiffness cannot attenuate direct disturbances over the same frequency band.

From a vibration engineering viewpoint, an alternative means of achieving rejection of disturbances is to fasten the experiment rigidly to an inertial structure. While there is no such structure in space, it is possible to achieve this effect by high gain feedback on inertial experiment position. This inertial position feedback acts like a very stiff spring tying the

experiment to inertial space. While such a controller may meet the 0.1 Hz 40 dB specification, it will not satisfy the specification on unit transmissibility [12]. If an inertial position feedforward loop is added, this problem can be eliminated. However, this method would be difficult to use effectively for multiple–degree–of–freedom isolation.

Another method of fastening the experiment to inertial space examined by the University is the use of inertial damping via feedback. By feeding back the inertial experiment velocity with a high gain it was shown for an example problem that it is almost possible to achieve both the 40 dB and the unity transmissibility specifications without resorting to feedforward. Unfortunately, the roll–off rate is approximately 20 dB/decade, so that both specifications can not be simultaneously achieved [12].

Another passive analogy examined was the lowering of the natural frequency of the umbilical by increasing the experiment mass. An increased experiment mass would attenuate direct disturbances as well as those transmitted through the umbilical. In addition, at frequencies below the natural frequency of the umbilical–mass system, the isolation system would have unity transmissibility. Of course, for space applications any additional mass is very costly. To lower the natural frequency by an order of magnitude would require increasing the experiment mass by a factor of one hundred. Clearly, it is not practical to accomplish increased isolation through the addition of real mass. However, it is possible to increase the effective mass of the system through feedback [12].

To summarize, the passive isolation analogies examined yield some insight but they fall short as design approaches on three counts: (1) they do not have flexibility to shape the response so as to achieve the performance requirements, (2) they cannot be easily generalized to multi–degree–of–freedom problems, and (3) they completely ignore the robustness problems inherent with active control systems.

4.3 Classical Control Design

A one–dimensional isolation problem, shown in Figure 7, was examined using a classical controls loop–shaping approach, to gain insight into controller design and limitations. System

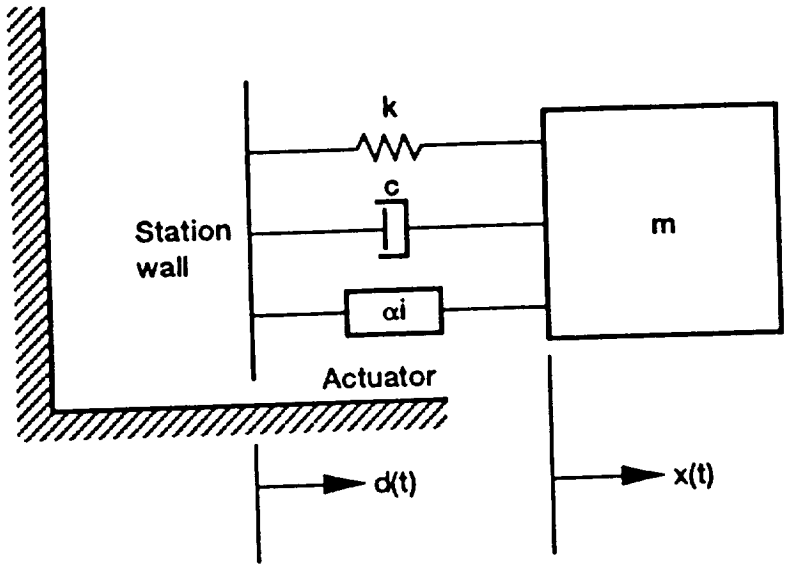

Figure 7: One–dimensional isolation problem

parameters were chosen to be representative values which yielded a low natural frequency ($k/m = 0.1$, $\omega_n \approx 0.05$ Hz [0.316 rad/sec]), and damping was assumed light ($\zeta = 0.1$). In the following discussion the variables d, x, and u represent experiment rack position, payload position, and control force, respectively; and it is assumed that the only available measurement is payload acceleration. The problem is to design a feedback controller, satisfying the following specifications:

1. Above 0.1 Hz the payload acceleration $\ddot{x}(t)$ should be 40 dB below the spacecraft acceleration $\ddot{d}(t)$.
2. Below 0.001 Hz the payload vibration x(t) should track the spacecraft vibration d(t) to within 10 percent, in order to prevent collision of the payload with the walls of the experiment rack surrounding it.
3. The payload should track perfectly the DC motion of the spacecraft, where no relative motion can be tolerated.

4. The loop gain of the system (plant and controller) should be less than 0.1 above 200 Hz, to avoid controller excitation of spacecraft– or payload flexible modes.
5. The payload acceleration should be less than or equal to 1.1 times the spacecraft acceleration at all frequencies.
6. Large phase margins should be attempted at all crossover frequencies.

The system equation of motion is

$$m\ddot{x} + c\dot{x} + kx = c\dot{d} + kd - u$$

and the system transfer functions are

$$s^2X(s) = \left[\frac{cs+k}{ms^2+cs+k}\right] s^2D(s) + \left[\frac{-s^2}{ms^2+cs+k}\right] U(s)$$

with a system block diagram as shown in Figure 8. R(s) represents the input disturbance (rack acceleration, Laplace domain), C(s) represents the payload acceleration, $H_1(s)$ represents the controller, and U(s) represents the control force. G(s) and $\frac{-s^2}{cs+k}G(s)$ are the two plant transfer functions, and H(s) is defined as indicated in Figure 8 for convenience.

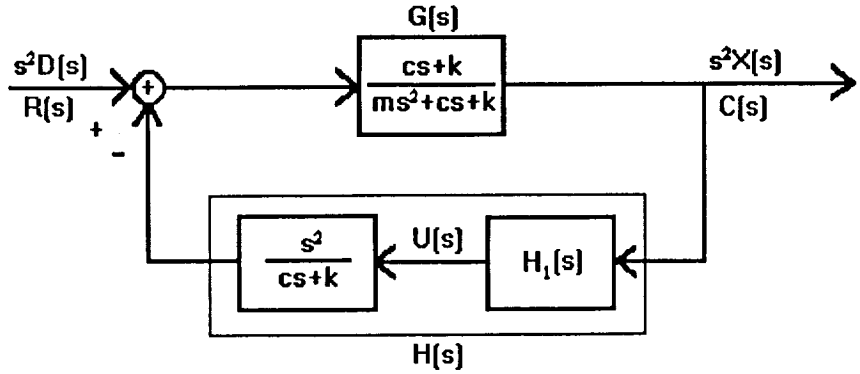

Figure 8: One–dimensional isolation system block diagram

The first five specifications can now be re–expressed, respectively, in the following form:

1. $\left|\frac{C(s)}{R(s)}\right| < 0.01$ above 0.1 Hz (0.628 rad/sec).

2. $0.9 < \left|\frac{C(s)}{R(s)}\right| < 1.1$ below 0.001 Hz ($6.28 \cdot 10^{-3}$ rad/sec).

3. $\lim_{s \to 0} \left|\frac{C(s)}{R(s)}\right| = 1.$

4. $|H(s)\, G(s)| < 0.1$ above 200 Hz (1256 rad/sec).

5. $\left|\frac{C(s)}{R(s)}\right| \leq 1.1$ for all frequencies.

In order to use the classical approach efficiently, the above specifications must be reduced to loop–gain form. This reduction yields, respectively, the following:

1. $\left|\frac{G}{1+HG}\right| < 0.01$ above 0.628 rad/sec, which in turn requires roughly that $|H| > 22$ (i.e., greater than 100/G1) at that point.
2. The second specification, $0.9 < \left|\frac{G}{1+HG}\right| < 1.1$ below $6.28 \cdot 10^{-3}$ rad/sec, is roughly equivalent (since $|G| \approx 1$ below ω_n) to the requirement that $|HG| < 0.1$ below $6.28 \cdot 10^{-3}$ rad/sec.
3. $\lim_{s \to 0} |HG| = 0.$
4. $|HG| < 0.1$ above 1256 rad/sec (same form as before).
5. $|HG| > 7$ in the vicinity of ω_n (where $|G| \approx 6.5$) to reduce the transmissibility to about unity in that region.

Standard loopshaping methods can now be used in a straightforward manner. See Figure 9 for asymptotic Bode–α plots of the specifications and of G(s); and for "first–pass" plots of the loop gain "L(s)" [i.e., H(s)G(s)] and of the controller $H_1(s)$.

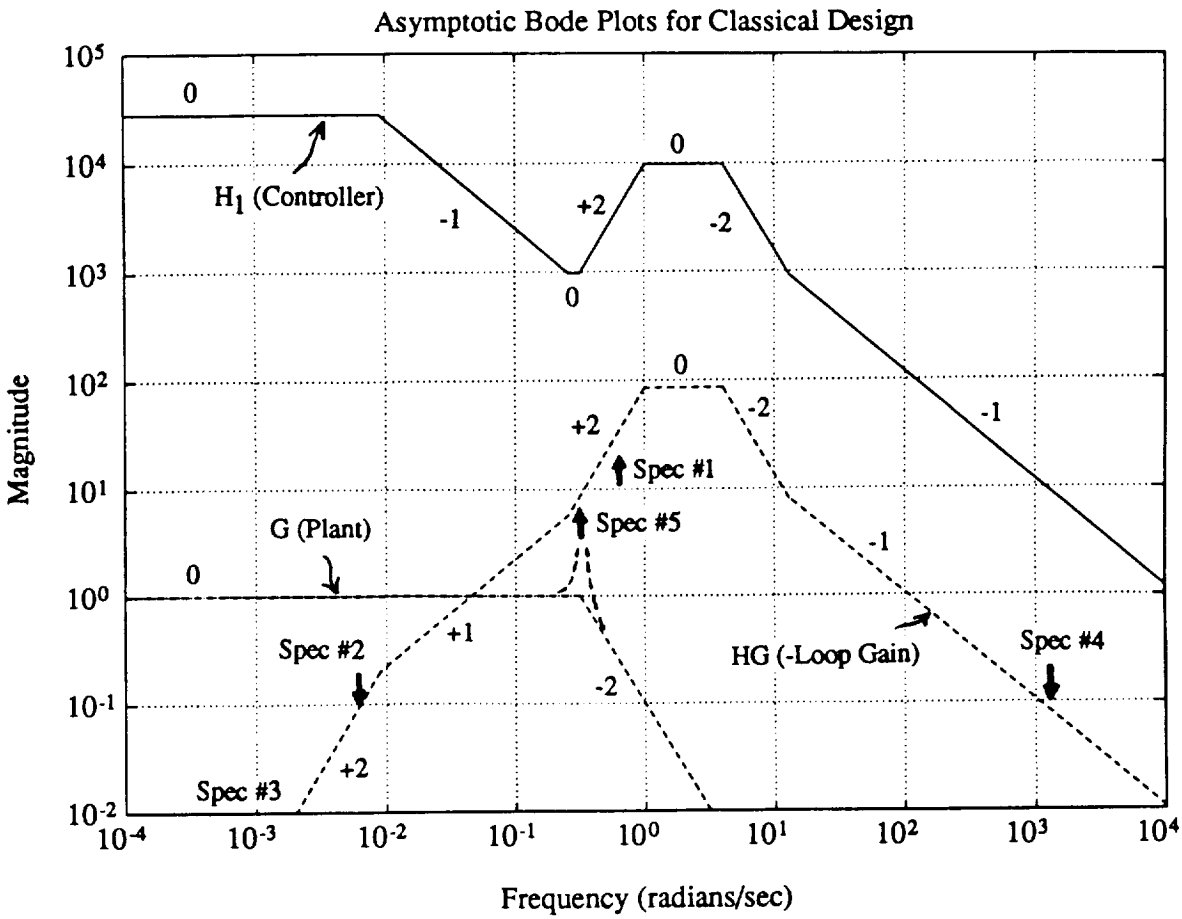

Figure 9: Asymptotic Bode–α plot of plant G(s) and "first–pass" loop gain L(s)

The controller developed first led to a transmissibility resonance at ω_n (not shown) so a filter of form $\frac{(s+0.316)^2}{s^2+0.1}$ was added, resulting in the following controller:

$$H_1(s) = \frac{1.2\cdot 10^3\ (s+0.25)(s+12)(s+0.316)^2(s^2+0.063\ s+0.1)}{(s+0.009)\ \ (s+1)^2\ (s+4)^2\ (s^2+0.1)}$$

Figures 10a,b,c represent loop gain, controller, and transmissibility plots, respectively. The control meets all specifications except for the goal of no more than a transmissibility of 1.1 at all frequencies; and this specification is almost met. The two phase margins associated with the above controller are 59^0 and 88^0, respectively.

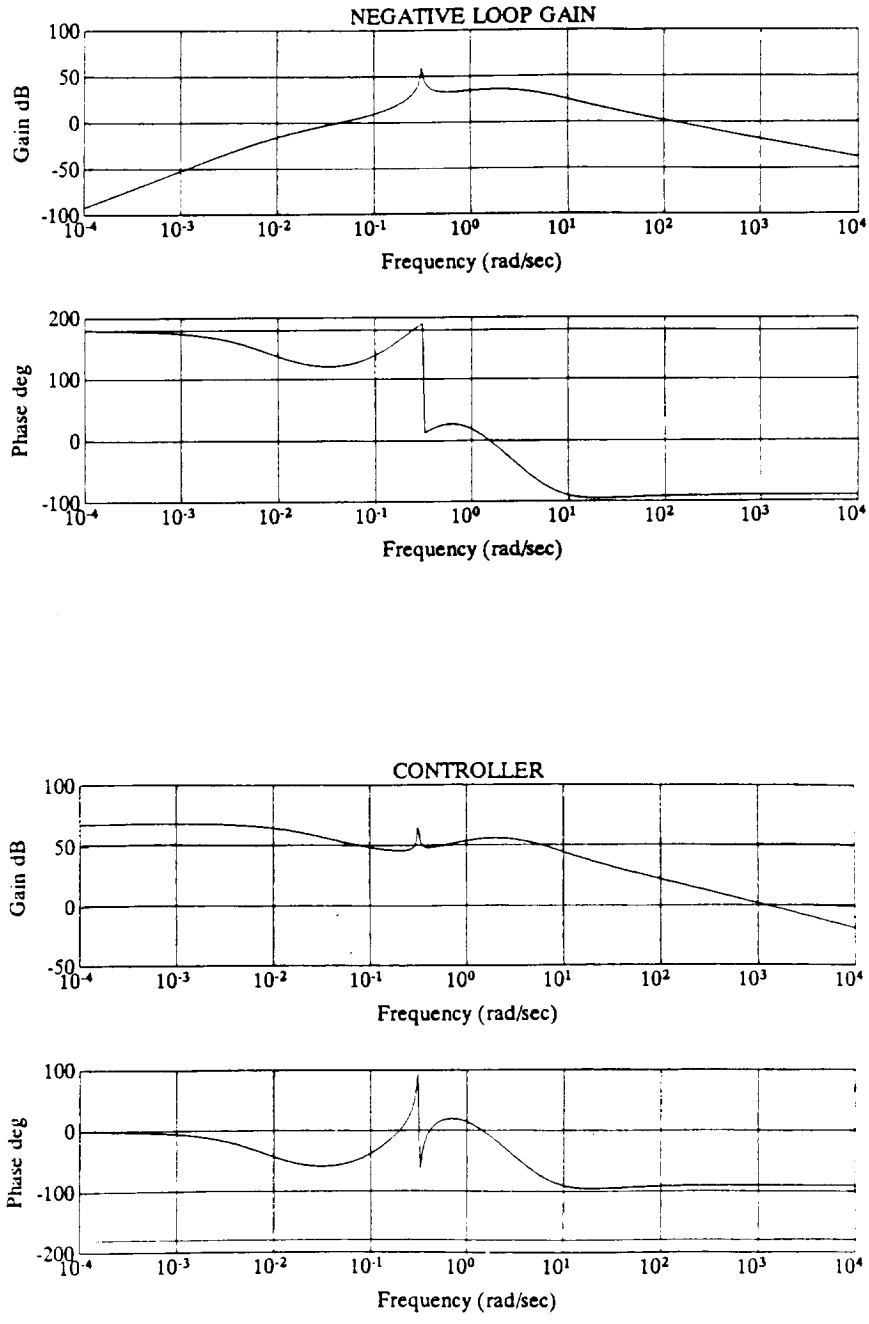

Figure 10: (a) Loop gain Bode plot, (b) controller Bode plot

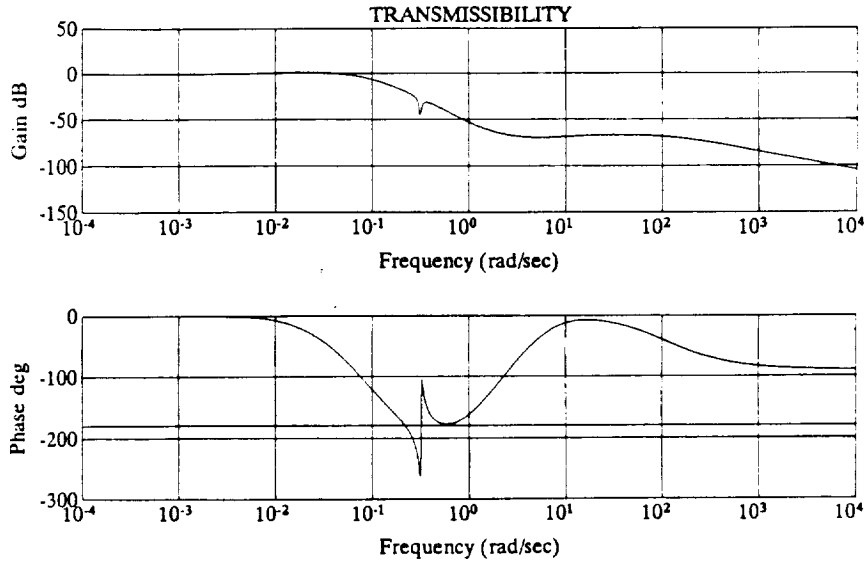

Figure 10: (c) Closed–loop transmissibility plot designed using classical control methods

From the above analysis the following conclusions can be drawn:

1. The requirement that $\left|\frac{C}{R}\right|$ be less than some fraction β_2 above some frequency ω_2 [spec #1] means that the open loop gain L(s) [i.e., H(s)G(s)] must be greater in magnitude than $\frac{1}{\beta_2}\left|G(s)\right|$ above ω_2. This means that there is a tradeoff between β_2 and PM_1. The smaller β_2 is, the smaller PM_1 can be. That is, the better the disturbance rejection above ω_2, the lower the achievable phase margin PM_1:
   $\beta_2 \downarrow \Rightarrow PM_1 \downarrow$. (Lowering β_2 will also tend to reduce PM_2, but not as directly.)
2. Raising ω_2 will improve PM_1 but degrade PM_2:
   $\omega_2 \uparrow \Rightarrow PM_1 \uparrow$, $PM_2 \downarrow$
3. The requirement to keep $|L(s)|$ below β_3 above ω_3 [spec #4] (so as to avoid exciting higher modes) has a cost in terms of PM_2 : $\beta_3 \downarrow \Rightarrow PM_2 \downarrow$.
4. Raising ω_3 raises PM_2: $\omega_3 \uparrow \Rightarrow PM_2 \uparrow$.
5. The requirement to hold $\left|\frac{C}{R}\right|$ within some fraction β_1 of unit transmissibility below some frequency ω_1 [spec # 2] means that $|L(s)|$ must be less than $\frac{1}{\beta_1}|G(s)|$ below ω_1. There is, then, a tradeoff between β_1 and PM_1: $\beta_1 \downarrow \Rightarrow PM_1 \downarrow$. (Changing β_1 does not significantly affect PM_2.)
6. Lowering ω_1 will improve PM_1: $\omega_1 \downarrow \Rightarrow PM_1 \uparrow$.
7. Lowering the natural frequency ω_n eases the difficulty in obtaining adequate PM_1 by lowering the constraint at ω_2 (see Figure 9) at ω_2: $\omega_n \downarrow \Rightarrow PM_1 \uparrow$. This means that reducing the physical umbilical stiffness or increasing the physical payload mass will make for an easier control problem.
8. The problem can be simplified, and both PM_1 and PM_2 can be increased, if the umbilical is damped such that the resonance near ω_n is small. (Refer to spec #5, p. 23.)
9. The controller need not have zero gain at DC to be acceptable, as long as
   $\lim_{s \to 0} s^2 H_1(s) = 0$. The controller may have a low frequency asymptote with slope -1, 0, or greater.

Although the classical approach is not readily extendable to the MIMO problem, it does provide some useful insights for informing the extended H_2 synthesis approach that we will examine in Section 5. Weighting $\ddot{x}(t)$ more heavily above ω_2 is analogous to lowering β_2 (see conclusion #1 above), so that better disturbance rejection is achieved at the expense of phase margin (esp. PM_1). Weighting the control u(t) more heavily at higher frequencies corresponds to trying to reduce β_3, so that a reduction in controller bandwidth is purchased at the expense of phase margin (PM_2) (see conclusion #3). At the lower end of the frequency spectrum, increased weighting of relative displacement (x–d), reduced weighting of absolute acceleration ($\ddot{x}$), or increased weighting of the control (u) each corresponds to attempting to lower β_1, at the cost of reducing PM_1 (see conclusion #5). Since an acceptable controller can have large, even infinite, DC gain (see conclusion #9) it is not necessary to weight u(t) highly at low frequencies. In fact for phase margin considerations (PM_1) it may be best to have "cheap" control at low frequencies, as previously noted (see conclusion #5). Unity transmissibility, then, could be "requested" at low frequencies by a relatively high low–frequency weighting of relative displacement.

4.4 Extending to the Multiple Degree–of–Freedom Problem

The University has extensively examined the design of multiple–input–multiple–output (MIMO) controllers for the multiple–degree–of–freedom active isolation problem. This work will be examined in detail in the next section. Here, we will introduce some of the problems of extending single–input–single–output (SISO) methods to MIMO problems by examining a simple multiple–degree–of–freedom benchmark problem [12], shown in Figure 11.

This problem illustrates how controller design via decoupling an isolation problem into its open loop modes, designing controllers for each mode, and recoupling back into the actuators, will often result in poor robustness due to unmodeled cross–couplings. This method of design, converting a MIMO control problem to a series of SISO problems, is often practiced. The example system is composed of an isolated platform (width 0.5 m and height 0.2 m, depth

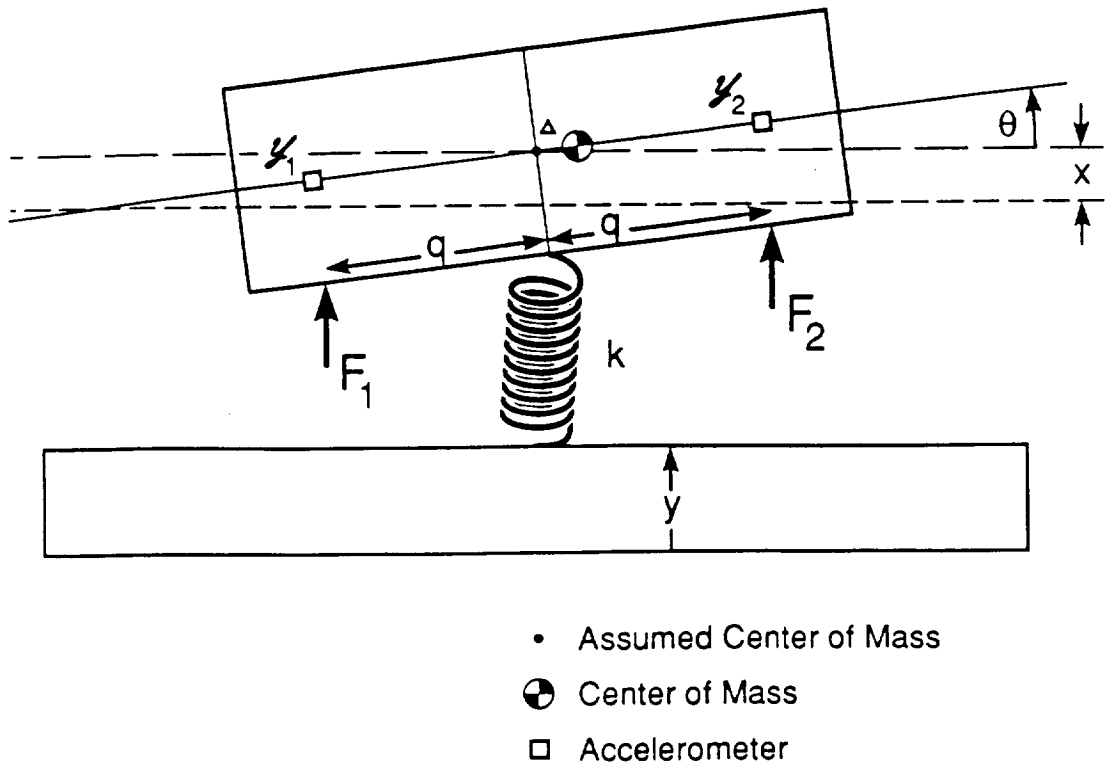

Figure 11: Simple multiple–degree–of–freedom benchmark isolation problem

unspecified), two accelerometers, two actuators, an umbilical, and a translating base. The platform may translate vertically or rotate about its center–of–mass. The actuators and accelerometers are positioned a distance of q = 0.2 m symmetrically about the assumed center–of–mass location. An umbilical of stiffness k (no damping) runs between this location and the base. The platform has mass m and inertia I. The equations of motion for the platform's translation x(t) and rotation $\theta(t)$ are

$$m\ddot{x} + k\Delta\theta + kx = f_1 + f_2 + d_1$$

$$I\ddot{\theta} + k\Delta^2\theta + k\Delta x = (q + \Delta)f_2 - (q - \Delta)f_1 + d_2$$

where d_1 and d_2 are the disturbances, and Δ is the error in the assumed center of mass. The

accelerometer readings are

$$y_1 = \ddot{x} - (q - \Delta)\ddot{\theta}$$

$$y_2 = \ddot{x} - (q - \Delta)\ddot{\theta}$$

The nominal system ($\Delta = 0$) can be decoupled in terms of the degrees of freedom by the change in variables

$$F = f_1 + f_2$$

$$M = q(f_2 - f_1)$$

$$z_1 = (y_1 + y_2)/2$$

$$z_2 = q(y_2 - y_1)/2$$

which are nominally the translational force, the moment, the translational acceleration, and the angular acceleration for the platform, respectively. The nominal transfer functions for the system are then

$$Z_1(s) = \left[\frac{s^2}{ms^2 + k}\right](F(s) + D_1(s))$$

$$Z_2(s) = \left[\frac{1}{I}\right](M(s) + D_2(s))$$

For translational motion, the natural frequency of the platform is $\sqrt{k/m}$. The rotational motion of the platform is free since the umbilical is attached to the center–of–mass. To compensate the nominal system, feedback can be designed for each mode of the system separately, since the system is decoupled. Translational acceleration and velocity feedback are first used to add effective mass and damping.

$$F(s) = -\left[a + \frac{c}{s}\right]Z_1(s).$$

This lowers the natural frequency of translational motion, yielding the closed loop transfer function

$$Z_1(s) = \left[\frac{s^2}{(m + a)s^2 + cs + k}\right] D_1(s).$$

Next, angular deflection feedback is used to constrain low frequency rotational motion and some damping is provided.

$$M(s) = -\left[\frac{n}{s} + \frac{b}{s^2}\right] Z_2(s)$$

yielding

$$Z_2(s) = \left[\frac{s^2}{Is + ns + b}\right] D_2(s)$$

where the control system values are in effective units. A control system was designed to lower the natural frequency of translational motion from 0.056 to 0.006 Hz with 40% of critical damping. The controlled rotational motion has a natural frequency of 0.006 Hz with 26% of critical damping. This controller design would yield very effective isolation on the nominal system.

The actual close loop poles, however, will be different from the nominal due to the error in the center–of–mass Δ. The poles of the actual system are given by the roots of the characteristic equation

$$[(m + a)s^2 + cs + k][Is^2 + ns + b] - [m\Delta][\Delta\{as^2 + cs + k)] = 0$$

For the nominal plant ($\Delta = 0$), this results in the prescribed natural frequencies and critical dampings. However, as the center–of–mass error increases, the poles migrate and the system becomes unstable. For an error as small as 6 mm for this system, instability occurs [12]. A plot of the pole movement vs. error in center–of–mass is shown in Figure 12. This sensitivity results from the ill–conditioned character of the designed controller. A proper MIMO

controller design might remedy this problem. In any case, an analysis of the problem from a MIMO control perspective would indicate the potential instability and the nature of the trade–off between performance and robustness.

In the next section, the MIMO design methods developed at the University of Virginia are examined in detail. Special attention is given to the issue of robustness.

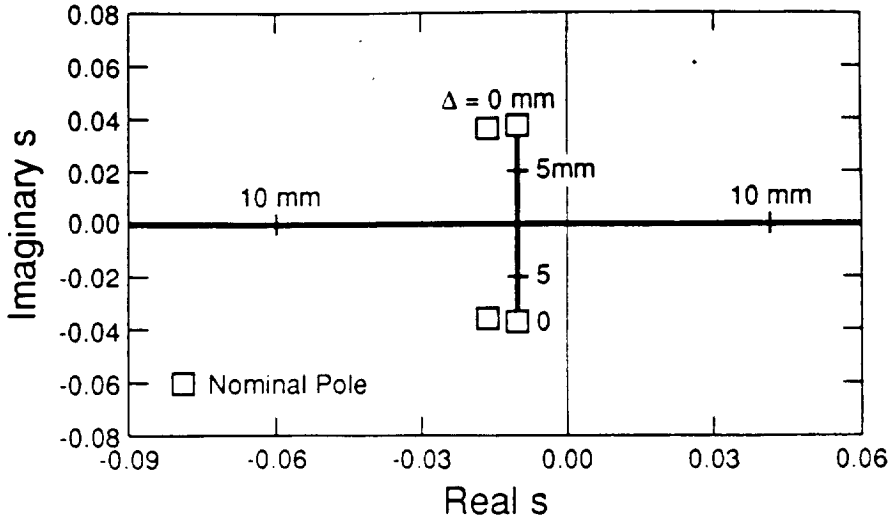

Figure 12: Loci of closed–loop poles as a function of center–of–mass error

5. MODERN CONTROL THEORY DESIGN

5.1 Modern Control Methods: An Overview

Researchers at the University have investigated the use of Linear Quadratic Regulator (LQR) and the Kalman–Bucy Filter (KBF) synthesis methods for the design of controllers for microgravity vibration isolation platforms [13,14,15]. The LQR method produces a state feedback controller which is optimal with respect to the quadratic (two norm) performance index

$$J = \int_{-\infty}^{\infty} \bar{x}^T(j\omega)Q\bar{x}(j\omega) + \bar{u}^T(j\omega)R\bar{u}(j\omega)\, d\omega$$

where Q and R are respectively the symmetric (usually diagonal) state and control weighting matrices, and $\bar{x}(j\omega)$ and $\bar{u}(j\omega)$ are the Fourier transforms of the state and control vectors. The state (positions and velocities for vibration isolation) satisfies the differential equation

$$\dot{x} = Ax + Bu$$

The quadratic performance index of LQR is well suited to this problem since vibration isolation quality is usually measured in terms of root–mean–square. However, it has been shown by researchers at the University that some modification of the performance function is necessary to apply this synthesis procedure to microgravity isolation controller design. State feedback for the isolation problem is feedback of experiment positions, velocities, angles, and angular velocities. Thus, LQR can only result in (inertial or relative) stiffness and damping feedback. As was discussed previously, these isolation techniques cannot yield acceptable isolation performance. Thus, an LQR performance index will not yield a satisfactory controller unless frequency weighted Q and R matrices are used, or the plant model is changed so as to have an acceleration pseudo–state [12]. Either of these methods results in the addition of pseudo–states to the state variable model. Frequency weighted Q and R matrices are also necessary to achieve robustness. Through choice of the weighting functions, the designer can, in essence, shape the control loops.

The differential equation above does not include a disturbance term. Consequently, the resulting controller is optimal with respect to white noise (a weakness of the LQR machinery). Since the power spectrum of the microgravity environment is not of this shape, the LQR controller will not be optimal with respect to rejection of the disturbance. Through the incorporation of a disturbance model (essentially a shaping filter), the LQR problem may be modified to yield an optimal disturbance accommodating (i.e. rejection) controller. This also incorporates the addition of pseudo–states to the state variable model. Disturbance accommodation may also aid in increasing the controller's robustness through loop shaping. Through the incorporation of the pseudo–states for frequency weighting and disturbance accommodation, controllers have been designed by University researchers using the standard Algebraic Ricatti equations of LQR–KBF. These calculations have been done using batch files written in the MATLAB language [15]. These controllers are then tested for robustness with respect to structured and unstructured uncertainties using singular value and structured singular value analysis. These analysis tools are the MIMO equivalent of the familiar gain margin, phase margin, and root locus robustness tests. Results for a one–degree–of–freedom problem are discussed below. MIMO vibration isolation research is ongoing at the University. These modern control methods require a considerable degree of skill and insight to employ properly.

5.2 Modern Control Results

The one–dimensional problem was first expressed in state–space form, with payload relative position, relative velocity, and acceleration selected as states. Although many other state choices could have been made, these three were chosen to minimize the number of states necessary and to maximize the physical intuition possible. The selection would result in a state feedback control that respectively modifies the effective umbilical stiffness and damping, and the effective payload mass—all being familiar, accessible, and intuitive system parameters. Relative, rather than inertial, position feedback would help to avoid exceeding

rattlespace limits; and relative velocity feedback would provide a means of damping out system resonances. The selection of acceleration as a state was considered desirable due to insight gained from the passive control studies. A controller which increases effective payload mass (by negative acceleration feedback) would potentially be able to accomplish disturbance rejection without unnecessarily sacrificing stability– or performance robustness.

A second important feature of the problem formulation was the decision to incorporate disturbances of two different kinds, the direct (i.e., onboard the experiment) and the indirect (i.e., acting via the umbilical). It had been observed that reducing the effective umbilical stiffness could aid in indirect disturbance rejection only, but that increasing payload effective mass could help reject disturbances of both kinds. Although the primary type of disturbance was considered likely to be the indirect, a means was needed to force the LQR–KBF (also known as LQG) "machinery" to increase effective mass so as to result in a robust controller. Including a direct disturbance provided this mechanism.

After completing the problem formulation, the next step was to develop a computer code for use in design and analysis. A PC–based design code was written in MATLAB to allow for accommodation of both direct and indirect disturbances. A large selection of frequency weightings and disturbance accommodation filters was made available to the designer. The code computes both feedback and observer gains, and also determines the constant feedforward (preview) gains for which the theory was developed in [16]. Although the feedforward option remains available, subsequent analysis determined that for the present application the feedforward gains do not make a significant enough contribution to warrant the additional controller complexity required. A number of analysis routines were also written to allow the designer to evaluate the resultant designs for purposes of comparison. The number of system states, system performance, stability robustness, parameter sensitivity, and observer quality are items whose comparisons are facilitated by these routines.

With the design and analysis tools in place, the next step was to develop the desired controller. In order to make the controller as simple as possible, it was decided to begin with

the basic LQG approach and to add complexity as needed. At each stage of additional complexity an iterative cycle of design and analysis was employed in an attempt to get the "best" achievable controller at that level of complexity.

The basic LQG approach (no frequency weighting, no disturbance accommodation, no direct disturbance) yielded a satisfactory controller in terms of performance; but it had almost no stability robustness to changes in umbilical stiffness from the nominal (as measured by feedback uncertainty). This lack of robustness was due to the fact that LQG found adding negative stiffness to be a "cheaper" means of indirect disturbance rejection than adding effective mass. No frequency weighting was found which could rectify this problem.

A direct white disturbance was added in an attempt to force the LQG design "machinery" to add effective mass. Although there were some gains in stability robustness this was due entirely to changes in observer gain matrix L. The feedback gain matrix K remained unaffected (note that this is fundamental in LQG theory and is not a numerical problem), and the feedback stability robustness was still unsatisfactory.

Disturbance accommodation, with a lowpass filter applied to a large direct (white) disturbance, resulted in a controller with excellent feedback– and multiplicative input stability robustnesses, as measured by singular value checks. The multiplicative output stability robustness was unacceptably low if cross–coupling was considered possible between states, but structured singular value checks indicated that without cross–coupling the allowable multiplicative output uncertainty was quite satisfactory. Since effective stiffness, effective damping, and effective mass of the controlled system are uncoupled for the true one–dimensional problem, the stability robustness measures of the system were considered acceptable. Further, the performance was excellent, easily exceeding the specifications. However, the controller gains were still large at higher frequencies where unmodeled system modes were of concern (see specification #4). It was therefore necessary to use state– and control frequency weighting in an attempt to force the controller to turn off by approximately 100 Hz (i.e., to reduce loop gain below a magnitude of one) so as to avoid exciting unmodeled

flexible modes. To reduce the loop gain at the higher frequencies it was necessary in that range (1) to place a high weight on control, (2) to apply low weights to all three states, and (3) to reduce the direct disturbance.

At low frequencies the control weighting was left constant (i.e., "flat"), in an attempt to minimize the number of added pseudostates. However, the resulting closed loop system now had very poor low frequency stability robustness to parametric uncertainties, even though it both retained its excellent performance and now provided the desired low controller bandwidth.

A classical design approach to the problem provided a simple solution to the robustness issue. It was noted that for a controller with acceptable nominal performance the low frequency asymptote for controller gain could have slope –1 or 0 or greater (Bode–α, log–log scale). Therefore, the control weighting at DC could be zero (filter slope ≥ 0) and the extended H_2 synthesis "machinery" could be freed to consider finite or infinite DC controller–gain options. This results, however, in the addition of a pseudostate. This change yielded a controller that satisfied the design specifications and exhibited good stability robustness to parametric and to multiplicative input– and output uncertainties. Considering (for the moment)only single–parameter uncertainties, stability was guaranteed for umbilical stiffness to within $\pm$99.7% of nominal, and umbilical damping could be essentially unknown. Payload mass needed to be known only to within $\pm$65.2% of nominal. Having these initial favorable indicators of system robustness the next step was to reduce the controller size. Further robustness analysis would then be conducted on the reduced–order controller.

The controller described above was a ninth–order controller (i.e., had nine states), with payload acceleration as its only required input. Other states and pseudostates were reconstructed in the observer. To reduce the controller to a smaller order, a routine was written in MATLAB in order to permit removing high frequency modes (modal truncation) and weakly controllable and –observable system dynamics [17]. The result of applying this to the ninth–order controller was a third–order controller that has all the essential features of the ninth–order one. The loop gain, controller, and transmissibility plots for this reduced

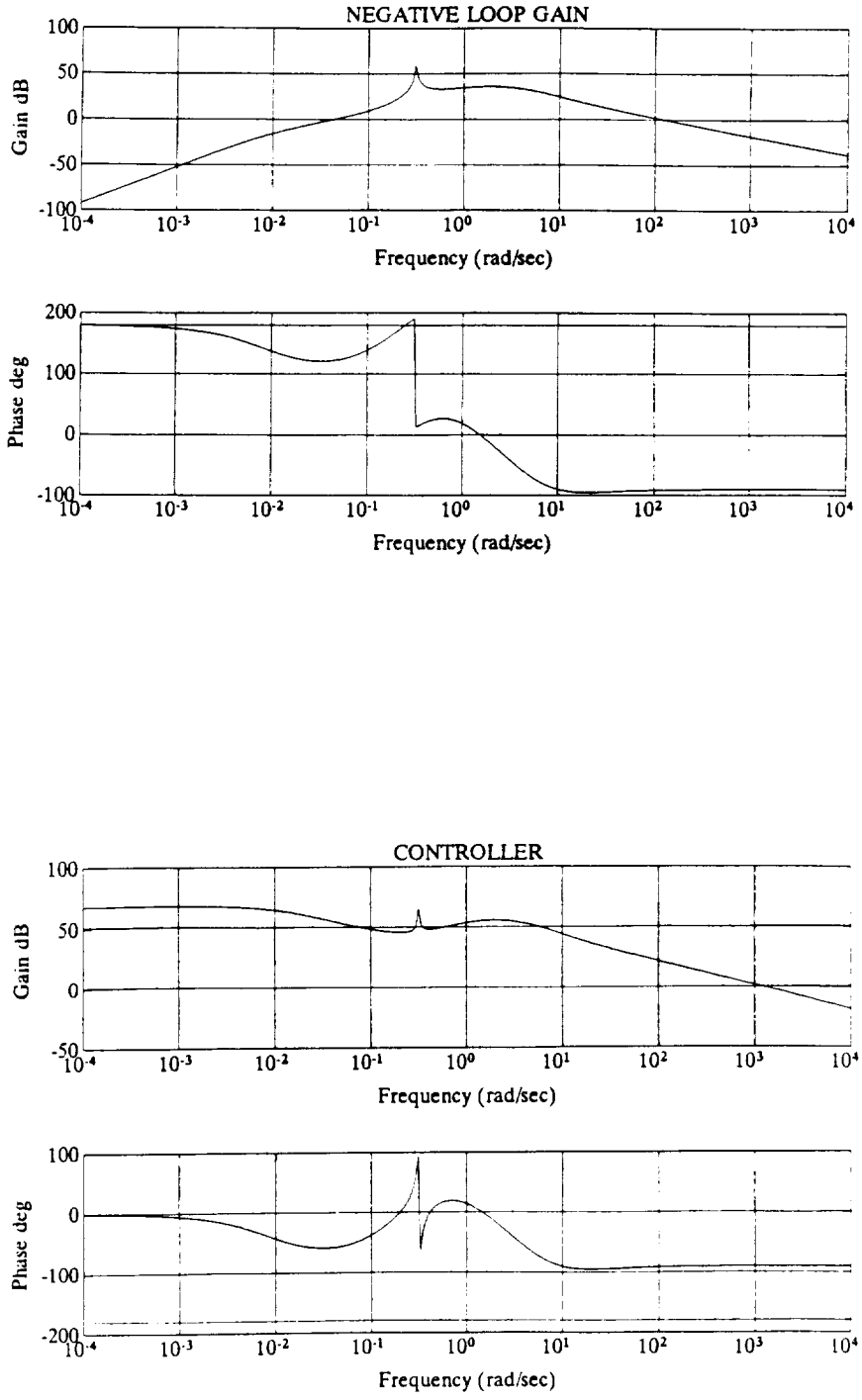

Figure 13: (a) Loop gain Bode plot, (b) controller Bode plot

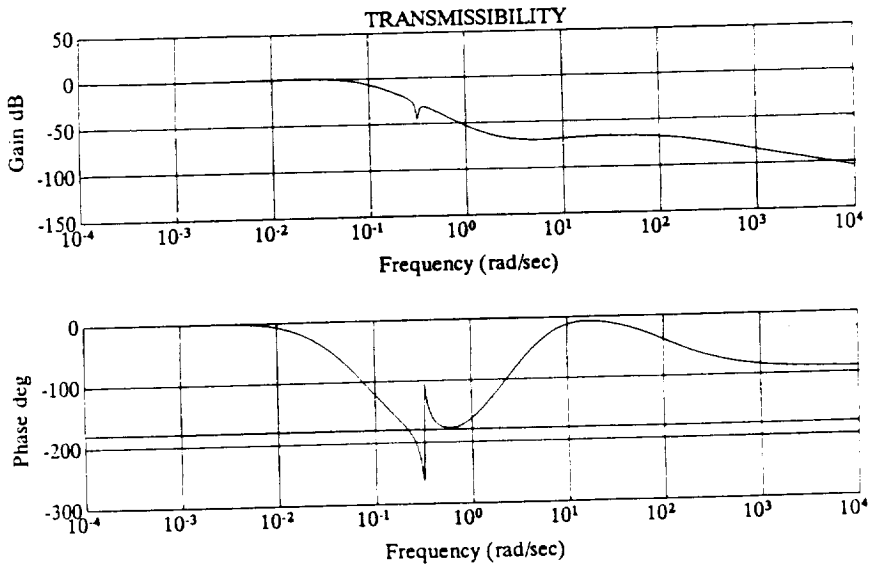

Figure 13: (c) Closed–loop transmissibility plot of system designed using extended H^2 synthesis

controller are shown in Figures 13a,b,c. Note from the transmissibility plot that the transmissibility is unity up to 10^{-3} Hz and that it is below 10^{-4} at 0.1 Hz. Notice further that the open loop and closed loop Bode plots merge at about 100 Hz. This is due to the fact that the controller has essentially "turned off" by that frequency (see Figure 13b).

There are four basic checks that must be made of any controlled system: nominal stability, nominal stability, robust stability, and robust performance. These four checks are considered below, consecutively.

The extended H_2 synthesis method used for this portion provides an inherent guarantee of stability for a nominal plant with full state feedback. Further, the "separation principle" guarantees that for a perfectly known plant a stable asymptotic observer will not destabilize the system. Thus, nominal stability is assured with the full order observer, provided the observer itself is stable. Reducing the controller order removes this guarantee, but simple eigenvalue checks verify that both the reduced third–order controller as designed and the associated controlled system are stable for the nominal plant. A simple check of the loop gain Bode plot (Figure 13a) confirms the conclusion that the closed loop system is stable, since it is known that the loop gain is minimum phase.

The second necessary check is of nominal performance. As indicated by the closed–loop transmissibility plot (Figure 13c) the nominal performance is quite satisfactory. Note that the "less than 10^{-2}" spec at 0.1 Hz is surpassed by more than an order of magnitude. This overdesign was intentional, and necessary, since plant modeling errors (open loop system, sensors, and actuators) will certainly degrade performance margins.

Robust stability measures are necessary to determine whether the closed–loop system will remain stable given the anticipated sensor, actuator, and plant parameter uncertainties. Three different types of robust stability measures were used, for guaranteeing system stability for multiplicative input, multiplicative output, and feedback uncertainties below certain levels. The multiplicative input uncertainty allowable was found to be equivalent to a guaranteed phase margin (interval) of [–48°, +48°], and to a guaranteed gain margin (interval) of [0.304,

5.434]. The actual margins are even larger (phase margins: [–55°, +55°], gain margins: [0,+∞]). Since only one plant output is sensed (viz., payload acceleration), the multiplicative input and output robust stability guarantees are identical. A feedback uncertainty measure was used to determine guaranteed minimum stability bounds on uncertainties in umbilical stiffness and damping, and on payload mass. It was found, as noted previously (p. 34), that closed–loop system stability was guaranteed for single–parameter uncertainties much larger than anticipated. By considering the feedback uncertainty structure, it was shown that for simultaneous mass, damping, and stiffness uncertainties of ±20%, ±100%, and ±69%, respectively, system stability could be assured. Higher frequency modes of the system were considered not to be a significant concern since the controller bandwidth was limited during design.

Finally, measures were needed of performance robustness. Structured singular value plots were made to find conservative bounds on multiplicative input (and output) uncertainties that would not lead to plants with unacceptable performance. Below 10^{-3} Hz it was found that for combined sensor and actuator uncertainties of up to ±11° in phase or of ±19% in gain the performance can be guaranteed to remain acceptable. At higher frequencies the guarantees are much better, so that by 220 Hz uncertainties of up to ±180° in phase or of ±200% in gain are permissible.

Structured singular value plots were also used in an attempt to find performance robustness guarantees in the face of known parametric uncertainties, but the effort was only partly successful. The checks led to the conclusion that for single–parameter uncertainties in stiffness of ±40% both stability and acceptable performance could be assured. However, single–parameter uncertainty bounds found by this method on damping and mass were too conservative to be useful. Consequently, real parametric studies were conducted on plant–uncertainty effects on closed–loop performance. It was determined that closed loop performance appeared acceptable for the various combinations of parametric uncertainties

6. EXPERIMENTAL RIG

6.1 Introduction

The University began construction of a one–degree–of–freedom experimental rig to demonstrate active microgravity isolation in the fall of 1990. The rig, now completed, was designed so as to illustrate active isolation of a tethered mass down to very low frequencies (0.01 Hz). This required both a large–stroke actuator and acceleration feedback as discussed in Sections 2 and 4. To our knowledge, this is the first microgravity rig to address either tethered or large–stroke active isolation.

6.2 Rig Description

The experimental rig built at the University of Virginia is shown in Figure 14. The rig consists of a 75 lb. steel cylinder representing a microgravity experiment, two air dashpots representing umbilicals, an electrodynamic shaker representing the vibrating experiment rack, and the large–stroke Lorentz actuator. The steel cylinder is suspended with magnetic supports so that it may freely move horizontally along its axis [16]. Similar to radial magnetic bearings, each support consists of four horseshoe electromagnets. Eddy current probes sense the radial position of the cylinder and complete the magnetic suspension feedback loops supplying current to the electromagnets. The supports hold the cylinder firmly in place but produce no friction. When the electromagnetic support system is turned off, the cylinder rests on a pair of touchdown pedestals.

The electrodynamic shaker (representing the experiment rack aboard the orbiter) has a long peak–to–peak stroke of 6.25 inches. This is the vibration source from which the steel cylinder (experiment) must be isolated. The shaker is mounted, via aluminum plates, on a concrete block resting on the laboratory floor. The shaker can generate sinusoidal, random or impulse waveforms at frequencies down to DC, thus simulating the disturbances typically produced on a manned orbiter.

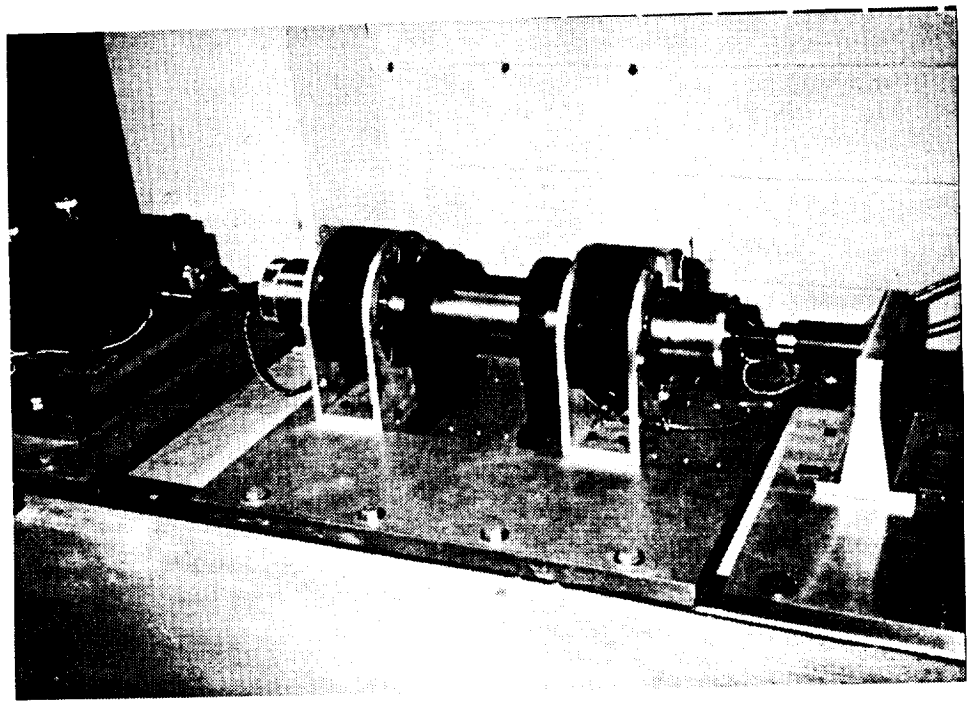

Fig. 14. Microgravity isolation rig at the University of Virginia

The umbilicals connecting a microgravity experiment to the orbiter are expected to be flexible hoses and wires. These are modeled by air dashpots with adjustable stiffness and damping coefficients. The vibration isolation test rig at the University has been designed so that different kinds of umbilicals may be employed, including actual hoses like those used for fluid transfer. The large–stroke Lorentz actuator connects the levitated steel cylinder to a plate connected to the concrete base.

The axial acceleration of the cylinder is sensed off a sensory plate using a very low frequency accelerometer with a resolution of approximately 1 μg. The accelerometer signal is fed through a low pass filter and a transconductance bipolar linear amplifier to produce the required current. This current is applied to the Lorentz actuator to isolate the cylinder from the disturbances generated by the shaker.

The background vibration levels on the concrete base on which the cylinder is mounted have been measured over several twenty–four–hour periods, in both the horizontal and the vertical directions. These vibrations are of the order of milli–g's, the quietest period occurring from late in the night to early in the morning [18]. Operating at this time will yield the highest degree of reproducibility in our results.

6.3 Experimental Results

Preliminary results have been obtained for vibration isolation in the (1–3) Hz range. An air dashpot (umbilical) was the only direct connection between the shaker armature (space platform) and the cylinder (science experiment requiring isolation).

An HP Structural Dynamics Analyzer was used for data acquisition. Figure 15 is a typical example illustrating the isolation obtained using simple lowpass acceleration feedback. The shaker generated a sinusoidal armature motion at a frequency of 2 Hz. For this case, the shaker's acceleration had an amplitude of 14,000 μg. The cylinder had a peak acceleration amplitude of approximately 7,000 μg with the controller "off" and 465 μg with the controller "on". Therefore, a fifteen–fold reduction of vibration has been obtained through acceleration feedback.

The control system is now being modified to improve the isolation capability of the controller.

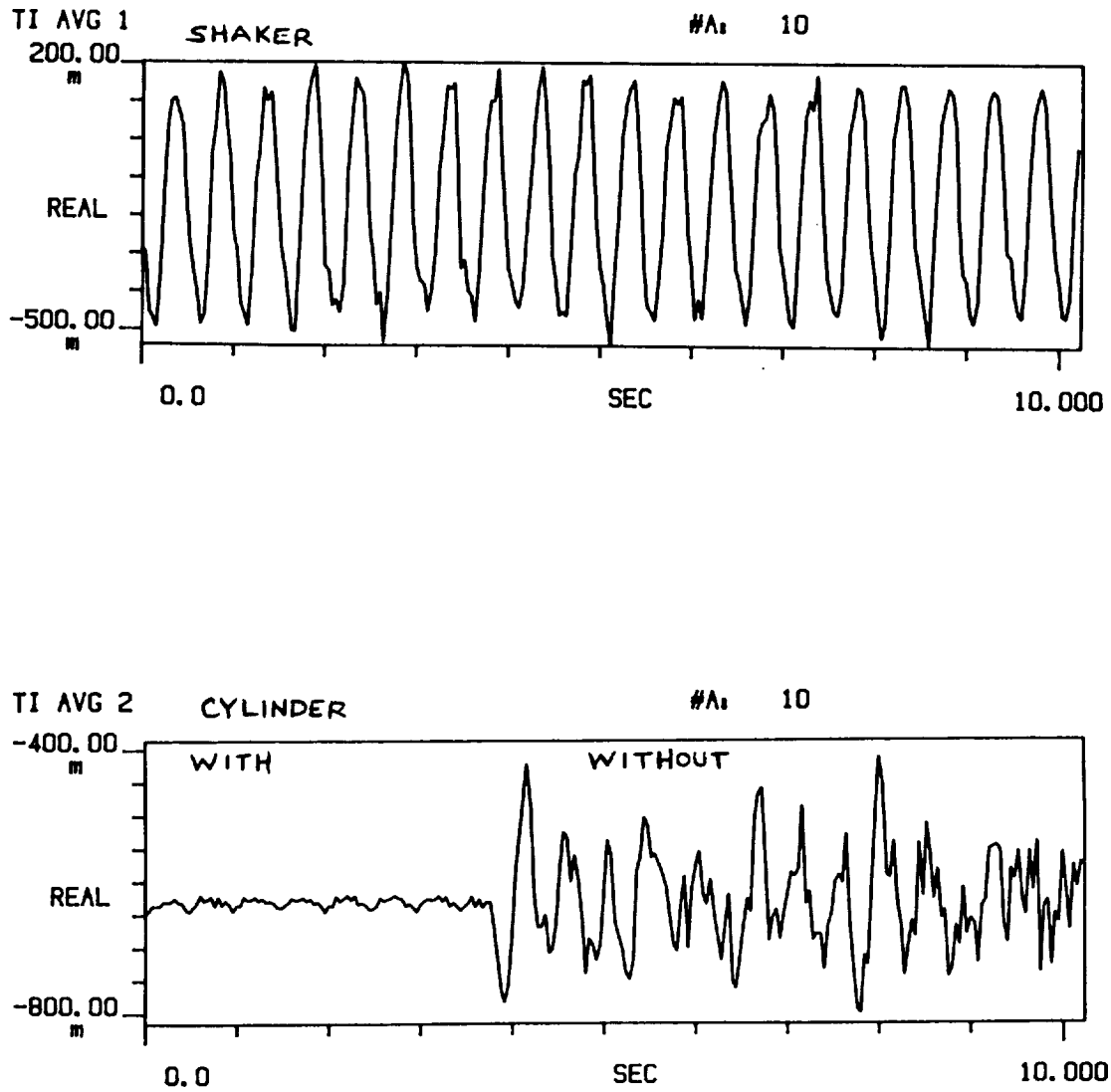

Figure 15: Shaker acceleration and cylinder acceleration with and without feedback control

experiment designers on the frequencies and amplitudes (or power spectrum) of allowable direct disturbances can be written. Such a specification would require that direct disturbances be acceptable without active vibration control for frequencies near and above the first flexible mode. This may help focus attention on the issue of direct disturbances and experiment design so that any required technology development may begin soon. For example, such a specification may result in the inclusion of passive vibration isolation mounts onboard the experiment package to isolate the sensitive process from high frequency direct disturbances produced by auxiliary equipment (e.g., pumps, fans, shutters, valves).

* **The isolation frequency and amplitude requirements of microgravity experiments and the microgravity vibration environment of the space shuttle and space station need to be better characterized.** This is very important in the low frequency (0–1 hz) range. Only when these quantities are specified can the required stroke of the actuator be determined. If strokes larger than 1 cm are necessary, a coarse–fine actuation system should be used. In this case, a technology development program needs to be started. The authors believe that a significant degree of development may be required for such a coarse–fine actuation scheme.

* **A six–degree–of–freedom microgravity isolation system needs to be flown aboard the space shuttle in the near future.** Only when we start developing actual hardware and software for an orbiting isolation system will we make significant progress toward practical isolation for space experiments. While we have learned a great deal from the experiments conducted so far, many of the difficulties that remain cannot be fully simulated or anticipated using ground based hardware.

7. CONCLUSION

The University has made substantial progress in many areas of active microgravity isolation in the last three years. We have primarily addressed the design of actuators and control systems for the active isolation of tethered experiments. In actuator research, our work has examined electrodynamic and electromagnetic actuators for single and multiple–degree–of–freedom isolation, and the use of coarse–fine systems for the practical extension of electromagnetic isolation to large strokes. For control system design, we have addressed performance limitations, robustness issues, and the use of H^2 methods for synthesis. Finally, we have constructed a single–degree–of–freedom test rig and demonstrated active isolation of a tethered mass through acceleration feedback. Our research is ongoing and several important results are still to be achieved. The University looks forward to continuing its work in microgravity vibration isolation and to continued collaboration with NASA Lewis Research Center.

To make a microgravity environment available for space experiments in the near future, we recommend the following:

* **The umbilicals to be used to service the experiments need to be identified and their properties need to be examined.** As the research conducted at the University over the last three years demonstrates, the difficulty of achieving a microgravity environment is very directly related to the umbilical's properties. For multiple–degree–of–freedom isolation, the uncertain coupling of degrees–of–freedom through the umbilical may present a challenge to controller design. For this reason, it is also recommended that controlled umbilicals be examined.
* **The issue of direct disturbances needs to be addressed.** Acceleration feedback, like that developed in our work, will be effective against direct disturbances as long as the frequencies of these disturbances are below that of the first flexible mode of the experiment structure. Perhaps a specification for

examined, with mass and stiffness varied in the intervals [–50%, +100%] and [–20%, +100%], respectively, and with damping varied by more than ten times its nominal value.

The above extended H_2 synthesis – μ analysis approach produced a controller that easily satisfies the competing demands of the posed 1–D microgravity vibration isolation problem. Further, unlike the classical approach, it is readily extendable for use on a 3–D problem. Frequency weighting and disturbance– accommodation were both found to be necessary if H_2 synthesis is to be used in involving the posed isolation problem. Their inclusion, along with a judicious choice of states, provides the designer with a powerful and intuitive set of weapons for his design arsenal. Disturbance accommodation of a direct disturbance model is necessary to force the H_2 synthesis machinery to avoid negative–stiffness solutions. The result was an actively controlled system that uses a "smart" form of acceleration feedback to overcome the robustness problems that commonly plague the basic LQG synthesis approach.

[1] B. B. Banerjee, C. R. Knospe, and P. E. Allaire. Compact Lorentz Actuator: Final Design. In *International Workshop on Vibration Isolation Technology for Microgravity Science Applications*, April 1991.

[2] C. R. Knospe and P. E. Allaire. Limitations on Vibration Isolation for Microgravity Space Experiments. *AIAA Journal of Spacecraft and Rockets*, 27(6):642–646, November–December 1990.

[3] C. R. Knospe and P. E. Allaire. Limits on the Isolation of Stochastic Vibration for Microgravity Space Experiments. *AIAA Journal of Spacecraft and Rockets*, 28(2):229–237, March–April 1991.

[4] A. P. Allan and . R. Knospe. A Six Degree–of–Freedom Actuator Design for Microgravity Vibration Isolation. In *Internal Workshop on Vibration Isolation Technology for Microgravity Science Applications*, April 1991.

[5] A. P. Allan and C. R. Knospe. A Six Degree–of–Freedom Magnetic Bearing for Microgravity Vibration Isolation. In *International Symposium on Magnetic Suspension Technology*, August 1991.

[6] Terry S. Allen, Douglas D. Havenhill, and Kevin D. Kral. FEAMIS: A magnetically suspended isolation system for space–based materials processing. In *Annual AAS Guidance and Control Conference*, Keystone, Colorado, February 1–5, 1986. Rocky Mountain Section, American Astronautical Society.

[7] D. I. Jones, A. R. Owens, and R. G. Owen. A microgravity isolation mount. *Acta Astronautica*, 15(6/7):441–448, 1987.

[8] Carlos M. Grodinsky. Development and approach to low–frequency microgravity isolation systems. Technical Paper 2984, NASA, August 1990.

[9] Ralph Fenn and Bruce Johnson. A six degree of freedom Lorentz force vibration isolator with nonlinear controller. In *International Workshop on Vibration Isolation Technology for Microgravity Science Applications*, Cleveland, Ohio, April 23–25, 1991. NASA Lewis Research Center.

[10] Ralph L. Hollis, S. E. Salcudean, and A. Peter Allan. A six degree–of–freedom magnetically levitated variable compliance fine–motion wrist: Design, modeling and control. *IEEE Transactions on Robotics and Automation*, 7(3):320–332, 1991.

[11] Kenichi Takahara, Tamane Ozawa, Hiroshi Takahashi, Shitta Shingu, Toshiro Ohashi, and Hitoshi Sugiura. Development of a magnetically suspended, tetrahedron–shaped antenna pointing system. In *22nd Aerospace Mechanisms Symposium*, Hampton, VA, May 4–6, 1988. NASA Langley Research Center.

[12] C. R. Knospe, R. D. Hampton, and P. E. Allaire. Control Issues of Microgravity Vibration Isolation. *Acta Astronautica*, Vol. 25, No. 11, pp. 687–697, 1991.

[13] R. D. Hampton and C. R. Knospe. Extended H2 Synthesis for Microgravity Vibration Isolation. In *International Workshop on Vibration Isolation Technology for Microgravity Science Applications*, April 1991.

[14] R. D. Hampton, C. M. Grodsinsky, P. E. Allaire, D. W. Lewis, and C. R. Knospe. Optimal Microgravity Vibration Isolation: An Algebraic Introduction. *Journal of the Astronautical Sciences*, 40(2): 241–259, April–June, 1992.

[15] R. D. Hampton and C. R. Knospe. Extended H2 Synthesis for Multiple–Degree–of–Freedom Controllers. In *International Symposium on Magnetic Suspension Technology*, August 1991.

[16] R. D. Hampton, C. R. Knospe, C. M. Grodsinsky, P. E. Allaire, and D. W. Lewis. Microgravity Vibration Isolation: Optimal Preview and Feedback Control, NASA TM–105673, May 19, 1992.

[17] R. D. Hampton, C. R. Knospe, C. M. Grodsinsky. Controller Design for Microgravity Vibration Isolation Systems, 43rd Congress of the International Astronautical Federation IAF–92–0969, August 28–September 5, 1992.

[18] B. B. Banerjee, C. R. Knospe, and P. E. Allaire. A Microgravity Vibration Isolation Rig. In *International Symposium on Magnetic Suspension Technology*, August 1991.